Large-scale colloidal synthesis of Cu_5FeS_4 compounds and their application in thermoelectrics

*Aijuan Zhang[1], Xingchen Shen[1], Zhi Zhang [3], Xu Lu[1], Wei Yao[1], J.Y. Dai[3], Qiufan Chen[1], Lijie Guo[1], Guoyu Wang[*2], Xiaoyuan Zhou[*1]*

[1]College of Physics, Chongqing University, Chongqing 401331, P. R. China.

[2]Chongqing Institute of Green and Intelligent Technology, Chinese Academy of Sciences, Chongqing 400714, P. R. China.

[3]Department of Applied Physics, The Hong Kong Poly technic University Kowloon, Hong Kong.

*Corresponding author: xiaoyuan2013@cqu.edu.cn; guoyuw@cigit.ac.cn

Abstract

We report, for the first time, a large-scale colloidal synthesis (CS) of non-stoichiometric Cu_5FeS_4 powers at different temperatures (493 K, 533 K and 553 K) followed by spark plasma sintering. It is found that the carrier density of CS samples exhibits four orders of magnitude higher than that of samples synthesized by traditional solid states reaction methods (SS). The higher carrier density in CS Cu_5FeS_4 yields enhanced electrical conductivity and power factor over a wide temperature range. As a result, a ZT value of 0.56 is achieved in Cu_5FeS_4 compound synthesized at 533 K during the colloidal synthesis process which is about 47% higher than that of the bulk SS counterparts. Moreover, these CS samples show better mechanical performance compared to the SS samples, demonstrating a great potential of bornite based compounds for thermoelectric commercial application.

Keywords: Cu_5FeS_4 nanocrystals, thermoelectric performance, colloidal synthesis, non-stoichiometry, carrier concentration

1. Introduction

Efficiency of thermoelectric materials is generally evaluated by the dimensionless figure of merit ZT ($ZT = S^2\sigma T/\kappa$), where S, σ and κ denote the Seebeck coefficient, the electrical conductivity and the thermal conductivity, respectively [1-3]. Highly efficient thermoelectric materials should exhibit high power factor $PF = S^2\sigma$ combined with a low thermal conductivity. However, achieving high ZT in thermoelectric materials has always been a challenge because these transport parameters are often entangled through carrier concentration. One cannot improve individual parameter without having adverse effect on other parameters. [4-6]. In order to balance these three interrelated parameters, excellent thermoelectric materials should possess carrier concentration (n) ranging from 10^{19} to 10^{21} cm^{-3} and a characteristic concentration of heavily-doped semiconductor [7].

There are two general strategies to improve ZT of a thermoelectric material: increasing numerator power factor ($S^2\sigma$) or reducing the total thermal conductivity. With regard to the first strategy, many approaches such as introducing band convergence [8-10], electron energy barrier filtering [11], quantum confinement effects [12] and using the resonant level [13] have been proved to be effective. Equally impressive gains have been obtained using the 'rattler' concept proposed by Slack [14, 15]; for example, using filling atoms in the skutterudites [16] to reduce the lattice thermal conductivity [17, 18]. Another effective way to decrease the thermal conductivity is point defect scattering by alloying with other elements [19, 20], which has been successfully demonstrated for thermoelectric materials in lead telluride, [21] Heusler compounds [22] and SiGe [23].

Recently, Cu_5FeS_4 (Eg = 1.25 eV) as a promising thermoelectric material with an ultra-low thermal conductivity has been reported by L. D. Chen etc. [24]. Cu_5FeS_4 exists as orthorhombic structure phase (space group Pbca, a=c=10.950 Å, b=21.862 Å) below 473 K, cubic structure phase (space group Fm3m, a=10.950 Å) at intermediate temperature between 473 K to 543 K and high-temperature cubic phase (space group Fm3m, a=5.49 Å) above 543 K. The high-temperature phase shows an anti-fluorite type structure that the ordered sulfurs constitute eight tetrahedrons, serving as good electrical transport framework, while the five Cu atoms, one Fe atom, and two vacancies randomly occupy the center of these sulfur tetrahedrons. The completely disordered distribution of Cu, Fe, and vacancies in bornite could largely interfere the thermal phonon transport and result in low thermal conductivity. The orthorhombic phase and intermediate temperature phase are the superstructure of high temperature phase [25-28], leading to the complexity of the phonon density of states in this larger unit cell volume and the

reduction of the total thermal transport. Up to now, bulk Cu_5FeS_4 synthesized through solid states reaction methods (SS) reported by L. D. Chen etc. exhibits low electrical conductivity~5.0 Sm^{-1} due to a low carrier concentration of 1.7×10^{16} cm^{-3} at 300 K, leading to a low thermoelectric power factor $S^2\sigma$. However, the lattice thermal conductivity is very low due to the strong phonon scattering by the intrinsic complexity and highly distorted crystal structure in the bornite, yielding a relatively high thermoelectric performance with a maximum ZT value of 0.38 at 700 K for the stoichiometric Cu_5FeS_4. Short of the above report, to the best of our knowledge, improvement in thermoelectric properties in bornite is rare.

It is worth noting that the above-mentioned bornite has been, so far, mainly synthesized by the SS method, which is time and energy consuming and typically needs several days to prepare a densified product. Besides, the grain size attained by SS is typically on the scale of several micrometers. It is well known that reducing the grain size is indeed a powerful method to greatly suppress the lattice thermal conductivity and thus improve the overall thermoelectric performance. In contrast, the colloidal synthesis (CS) followed by the subsequent compaction into dense samples has been widely used to successfully prepare thermoelectric nanocrystals [29]. A significant reduction in the thermal conductivity associated with the increased grain boundary density has been reported [2, 28, 29]. This, of course, assumes that the phonon mean-free path is reduced more compared to that of electrons. In addition, colloidal synthesis may be able to optimize the electric properties due to the presence of point defects introduced during the synthesis process. However, low outputs, typically ranging from several tens to several hundreds of milligrams, hinder the optimization of the parameters in subsequent compacting procedures. The possible variations in chemical composition and size in nanocrystals obtained from different batches would have an uncertain impact on the final TE properties. Thus, a quick and efficient processing approach in a manner adaptable to industrial production is desired to synthesize thermoelectric materials. In this scenario, CS method was particularly applied to synthesize Cu_5FeS_4 nanocrystals, yielding over gram-scale products for TE applications after a single one-pot reaction. On the other hand, it is believed that the impurity energy level in bornite Cu_5FeS_4 is shallow and the resultant thermal activation energy is small, giving rise to the possibility to efficiently tune the carrier concentration in Cu_5FeS_4[24].

In this study, for the first time, we report the large-scale colloidal synthesis of Cu_5FeS_4 nanocrystals (NCs) at different temperatures (493 K, 533 K and 553 K), yielding 5 g of product per run. The obtained Cu_5FeS_4 NCs were subsequently compacted into dense bulks through the spark plasma sintering. The

effect of different CS temperatures on carrier densities and the corresponding thermoelectric performance in Cu_5FeS_4 bulks was explored. The remarkable increase in the electrical conductivity was obtained due to the higher carrier concentration arising from the non-stoichiometry in CS samples. The resultant high *PF* combined with the ultra-low intrinsic thermal conductivity leads to a peak ZT value of 0.56 in Cu_5FeS_4 compound synthesized at 533 K during the colloidal synthesis, about 47% higher than that of bulk SS counterparts. This is the first example demonstrating that over 5 g of Cu_5FeS_4 nanocrystals can be synthesized by a single one-pot solution-processed reaction, and the first report on the enhanced thermoelectric properties of Cu_5FeS_4 based bulks made from non-stoichiometric nanocrystals via colloidal synthesis. In principle, this synthetic procedure is highly extendable; therefore, other binary, ternary, or quaternary nanocrystals could be possibly prepared through similar procedures for thermoelectric application.

2. Experiment procedure

2.1. Material and methods

$CuCl_2$ (98%), $Fe(acac)_3$ (99%), S powder (99.8%) and Oleylamine (OLA) (80%-90%) were purchased from Aladdin Reagent Co. Ltd. Ethanol (99.7%), hexane (97%), $N_2H_4 \cdot H_2O$ (85%) were purchased from Kelon Chemical Reagent Factory. All of the chemical reagents were used as received without further purification.

S powder 50 mmol (1.62g) was dissolved in 175 ml of OLA at 353 K in a round-bottomed flask under vacuum for about 6 h until a brown solution was formed. $CuCl_2$ 50 mmol (6.86g), $Fe(acac)_3$ 10 mmol (3.86 g) were weighed and mixed in 150 ml of OLA in a three-necked flask. Continuous nitrogen flow was used to remove water and oxygen during the whole reaction process. The solution was stirred for 6h at room temperature and then heated to 453 K in 5 min. Subsequently, the solution was kept at this temperature for another 10 min to get a brown dispersion. The former S/OLA solution was added into this three-necked flask containing the metal salts and OLA under nitrogen atmosphere. The reaction commixture turned dark as soon as these precursors were mixed. After mixing the metal and sulfur sources, the reaction temperature was elevated to 493 K, 533 K and 553 K respectively, in order to investigate the influence of synthesis temperature. When the reaction was completed, the flask was cooled to 333 K. The brown-black product was centrifuged at 8000 rpm for 5 min. The upper solution was discarded and the obtained NCs were washed with hexane and ethanol for 5 cycles until the NCs

could not be dispersed in hexane any more. In order to remove any organic ligands and impurity $Cu_{1.8}S$, the NCs were stirred in a mixture of hydrazine (please note that hydrazine should be handled with extreme caution due to its high toxicity) and hexane with volume ratio of 1:1 for 12 h until the NCs were easy to get into the hydrazine phase. This process was repeated for 3 cycles. The hydrazine-capped NCs were collected and vacuum-dried, and subsequently densified by spark plasma sintering (SPS) at 723 K for 5 min in a 10 mm diameter graphite die under a perpendicular direction compressive stress of 45 MPa in vacuum. The obtained SPS processed cylinders were cut and polished into bars with dimensions 8×2×2 mm^3 and cylinders with dimensions of 10 mm in diameter and 1 mm in thickness on diamond-wire cutting machine for electrical transport and thermal diffusivity measurements, respectively.

2.2. Structural and thermoelectric characterization

The powders pulverized from SPS bulks samples were used for Powder X-ray diffraction (XRD). The powder diffraction patterns were collected using PANalytical X'pert apparatus with Cu Ka radiation (λ=1.54056 Å). The morphology and microstructure were investigated using Field Emission Scanning Electron Microscopy (SEM, JSM-7800F, JEOL) and Transmission electron microscopy (TEM, JEOL 2100F) with energy dispersive spectroscopy (EDS). Inductively coupled plasma (ICP, Thermo Scientific Icap 6300 DUO) analysis was conducted to determine the chemical composition. The room-temperature Hall measurement was performed on a homemade apparatus under a reversible magnetic field of 1.0 T. Both Seebeck coefficient and electrical conductivity were measured simultaneously via a LSR-3 LINSEIS system under helium atmosphere at a temperature ranging from 300 K up to 690K. The thermal conductivity was calculated from $\kappa=DCpd$, where thermal diffusivity (D) was investigated by the laser flash method (Netzsch LFA-457), Cp is the specific heat measured in a differential scanning calorimeter (Netzsch, 404 F3) and samples density d is measured with Archimedes' method. Vickers hardness was tested on a Semi-automatic digital micro hardness tester (AHVD-1000XY).

3. Results and discussions

3.1. Structure and morphology

The photograph of surface-clean NCs is shown in the inset of Figure 1 (a), the typical yield of NCs is more than 5 g. Phase investigations were conducted on the as-prepared Cu_5FeS_4-493, Cu_5FeS_4-533 and Cu_5FeS_4-553 nanocrystals and powders pulverized from SPS bulks. As shwon in Figures 1 (a) and (b), all these diffraction peaks could be identified as the orthorhombic Cu_5FeS_4 structure (PDF: 42-0586) without presence of any impurity phase. The regrowth and coalescence of the NCs can be noted through

the X-ray diffraction analysis, where we find the full width half maxima (FWHM) of the diffraction peaks of SPS bulks are much narrower than that of the original NCs and some peaks appear, which indicate that the crystallinity is improved after SPS process. Table 1 displays the composition of the obtained bulk determined by inductively coupled plasma (ICP) analysis. The average chemical composition can be described as $Cu_{5.28}Fe_{0.82}S_4$, $Cu_{5.1}Fe_{0.89}S_4$ and $Cu_{5.26}Fe_{0.91}S_4$ for Cu_5FeS_4-493, Cu_5FeS_4-533, Cu_5FeS_4-553, respectively, indicating that these samples are copper rich and iron insufficient.

The morphology, size and dispersion of the as-prepared Cu_5FeS_4 nanocrystals synthesized at 493 K, 533 K and 553 K are shown in Figures 2a, b, c, respectively. It is obvious that the as-synthesized nanocrystals are of non-uniform shape with size ranging from tens nanometers to several hundred nanometers. Such observation is different from previously reported colloidal synthesis of Cu_2ZnSnS_4 nanocrystals [2], where the obtained nanocrystals, with an average diameter of 25 nm, are nearly monodisperse, and most of the nanoparticles display cube-like morphologies. In addition, it is noted that the size of nanocrystals increases with increasing CS temperature. SEM images of fractured surfaces for Cu_5FeS_4-493, Cu_5FeS_4-533 and Cu_5FeS_4-553 bulk are displayed in Figures 2d, e, f, respectively. It is apparent that there are coalescence and regrowth of nanocrystals after SPS at even 493 K. The size of some coalesced nanoparticles can be up to 1 μm, but there are still a number of nanoparticles remained the original size, leading to a formation of hierarchical morphology in Cu_5FeS_4 bulk. This is considered as an advantage to reduce the lattice thermal conductivity. In addition, it depicts that there are some voids in these bulk materials and the number of voids decreases with the increase of the CS temperature. It should be pointed that all of the materials pellets are mechanically strong enough to endure the dicing and polishing process.

To understand the morphology and structural characteristics of the SPS-processed samples, detailed TEM investigation was conducted for Cu_5FeS_4-553 sample. Figure 3a shows a typical bright- field TEM image of the sample, from which many grains can be clearly observed. Selected area diffraction pattern (SAED) was used to determine their crystal structure, and Figure 3b is a typical SAED pattern. Our detailed analyses of the SAED patterns indicate that the sample belongs to the orthorhombic phase Cu_5FeS_4. Figure 3c is an enlarged TEM image where one can see that many small grains with the dimension around 20 nm are embedded in large particles. Figure 3d is a high-resolution TEM image taken from the marked area in Figure 1c, and it can be noticed that the lattice spacing matches well with

the orthorhombic phase Cu_5FeS_4.

3.2. Influence of CS temperature on thermoelectric properties

The temperature dependence of electrical transport properties (σ, S and PF) is plotted in Figure 4. As shown in Figure 4 (a), the electric conductivities of these CS samples fall in the ranges of 4983 – 12889 S/m and 11661 – 16566 S/m at room temperature and 690 K, respectively, which are larger than those of previously reported Cu_5FeS_4 SS bulk at the given temperatures [24]. The enhancements in the electric conductivities can be attributed to the non-stoichiometry in the CS samples. To be specific, Cu-rich and Fe-poor as indicated in Table 1. Assuming that the stoichiometric Cu_5FeS_4 is a charge-balanced semiconductor with 8 electrons from cations and 8 holes from anions, one can conclude from the ICP data that the CS samples have less electrons, leading to their p-type behavior and increased hole concentration. Obviously, the carrier concentration of CS bulks is 3~4 orders higher than that of SS bulk [24]. Apart from this, samples synthesized at higher CS temperatures have more electrons based on the ICP data, which is also consistent with the fact that the hole concentration decreases with the increase of CS temperature. The values of carrier densities are estimated to be 2.6×10^{20}, 1.5×10^{20}, 1.4×10^{20} and 1.7×10^{16} cm^{-3} for Cu_5FeS_4-493, Cu_5FeS_4-533, Cu_5FeS_4-553 and SS bulk, respectively. Thereby, as demonstrated in Fig. 4(a), the electrical conductivity for CS bulks is much larger than that of SS bulk and decreases with increasing the CS temperature. The electric mobility (ν) was calculated according to the formula $\sigma = ne\nu$. Meanwhile, it is interesting to note that the mobility of CS bulks is in the range of 3.1 - 2.2 $cm^2V^{-1}s^{-1}$ and decreases with decreasing carrier concentration. A clear reason for this temperature dependence is not clear at the present stage, a possible issue however pertinent is the increasing amount of magnetic ions (Fe^{3+}) in CS bulks. Figure 4(b) shows that all CS samples have a positive Seebeck coefficient, indicating that the majority carriers are holes. It is worth noting that SS bulk exhibits n-p transition, indicating a majority carrier shift from n-type to p-type semiconductor at 450 K [24]. Besides, the Seebeck coefficient of CS samples is significantly lower than that of the SS sample. This trend is in good agreement with that reported in literatures [2, 29]. Such reduced Seebeck coefficient can be ascribed to the raised carrier density in CS bulks. In contrast to the Seebeck coefficient of 190 μV/K at 690 K for SS bulk, the Seebeck coefficients of 183,170, and 161 μV/K were obtained for Cu_5FeS_4-493, Cu_5FeS_4-533 and Cu_5FeS_4-553, respectively. The highest power factor is obtained for Cu_5FeS_4-493, reaching its maximum of 0.43 $mWK^{-2}m^{-1}$ at around 690 K, which is about 70% higher than that of SS bulk [24].

The temperature dependence of total thermal conductivity κ, the carrier thermal conductivity κ_e and lattice thermal conductivity κ_l are shown in Figure 5a, Figure 5b and Figure 5c, respectively. All these samples exhibit ultra-low thermal conductivity over the entire measured temperature range. The values of the room temperature thermal conductivities for Cu_5FeS_4-493, Cu_5FeS_4-533, Cu_5FeS_4-553 and SS bulk are respectively 0.64 $Wm^{-1}K^{-1}$, 0.475 $Wm^{-1}K^{-1}$, 0.402 $Wm^{-1}K^{-1}$ and 0.385 $Wm^{-1}K^{-1}$. One may notice the variation of the thermal conductivity, i.e., it first decreases with increasing temperature, and afterwards, increase with an inverse trend. This variation is consistent with the phase transition from the intermediate temperature phase to the high temperature phase occurring at 525 K for Cu_5FeS_4-553, Cu_5FeS_4-533 and 475 K for Cu_5FeS_4-493. On the other hand, it is apparent that the total thermal conductivity increases when lowering the CS temperature; this can be partially attributed to the raised κ_e due to the rising carrier density as well as the increased lattice thermal conductivity for CS bulks. The total thermal conductivity, $\kappa = \kappa_e + \kappa_l$, can be divided into two major components: the carrier component κ_e is due to the heat transported by electrons and the lattice component κ_l is due to the heat transported by phonons. The carrier thermal conductivities were obtained via the Wiedemann-Franz relationship, $\kappa_e = L\sigma T$, where L is the Lorenz number, σ is electrical conductivities and T is absolute temperature. The Lorenz number was calculated based on the Mott equation found elsewhere [21]. The lattice thermal conductivities were calculated by subtracting the carrier thermal conductivities from the measured thermal conductivities. As to the lattice thermal conductivity, similar to bornite SS bulk, these CS materials remain relatively intrinsic low lattice thermal conductivity due to the strong phonon scattering by the intrinsic complexity and highly distorted crystal structure in the bornite compound. To be specific, at room temperature, the values of κ_l are 0.38 $Wm^{-1}K^{-1}$, 0.44 $Wm^{-1}K^{-1}$ and 0.56 $Wm^{-1}K^{-1}$ for Cu_5FeS_4-493, Cu_5FeS_4-533 and Cu_5FeS_4-553, respectively. Besides, the lattice thermal conductivity demonstrates the same behavior as the total thermal conductivity. Due to the phase transition, the minima of the lattice thermal conductivity are reached at 525 K for Cu_5FeS_4-533 and Cu_5FeS_4-553 and 475 K for Cu_5FeS_4-493. In addition, it is worthy to mention that, in this work, the lattice thermal conductivity of CS bulks is larger than that of SS bulk as reported by L. D. Chen's group. Specifically, at room temperature, the lattice thermal conductivity increases from 0.2 $Wm^{-1}K^{-1}$ for SS Cu_5FeS_4 bulk to 0.56 $Wm^{-1}K^{-1}$, 0.44 $Wm^{-1}K^{-1}$ and 0.398 $Wm^{-1}K^{-1}$ for Cu_5FeS_4-493, Cu_5FeS_4-533 and Cu_5FeS_4-553 CS bulks, respectively. Such difference is opposite to our expectation since CS bulks are believed to show lower lattice thermal conductivity due to the enhanced phonons scattering from the hierarchically structure in CS bulks as observed via TEM

[30].

Figure 5d shows the temperature-dependent dimensionless figure of merit *ZT*, where the peak *ZT* values of Cu_5FeS_4-493, Cu_5FeS_4-533 and Cu_5FeS_4-553 are 0.43, 0.51 and 0.56 at 690 K, respectively. As compared to the bornite SS bulk, CS bulks possess much higher *ZT* over the whole measurement temperature [24]. The improved thermoelectric performance of CS samples mainly results from the high electrical conductivity caused by the four orders of magnitude increase in carrier density as well as the intrinsic low thermal conductivity in spite of the relatively raised total thermal conductivity. Besides, compared to the previously reported solid state synthesis of Cu_5FeS_4-based materials, the synthesis temperature of our procedure (493-553 K) is much lower, and the reaction time is dramatically shortened to less than one day. Consequently, the synthetic strategy developed here is absolutely competitive among the entire energy saving technology. Further improvement in ZT of Cu_5FeS_4 based materials could be obtained by: 1) optimizing wet-chemistry parameters to synthesize nanocrystals with uniform and much reduced grain size; 2) Manipulating SPS procedure to obtain much sharper and cleaner grains as well as grain boundaries in the final densified bulk, thereby promoting charges transport and increasing carriers mobility; 3) properly doping to simultaneously improve carriers density and/or to seek potential resonant states in Cu_5FeS_4 based materials to greatly enhance Seebeck coefficient while maintaining the electrical conductivity.

Apart from the enhanced thermoelectric performance, it is interesting to note that these CS bulks show better mechanical robustness as compared to SS bulk. The Vickers hardness (HV) of Cu_5FeS_4-493, Cu_5FeS_4-533, Cu_5FeS_4-553 samples and Cu_5FeS_4 SS bulk is characterized under 50 g load and maintained 10 s at room temperature. Area of indentation can be obtained by atomic force microscope, and HV is determined by Equ. 1

$$\mathrm{HV} = 0.102 \times \frac{F}{S} = 0.102 \times \frac{2F \sin\frac{\alpha}{2}}{d^2} \qquad (1)$$

where F is the load pressure, S is the residual rhombus area, α = 136 ° is angle of the rhombus, d is the average diagonal length of the indentation. The HV values of these materials are displayed in table 1. Due to the fact that the SS bulk is too brittle, the exact HV value of SS bulk can not be obtained. The HV values for CS bulks for Cu_5FeS_4-493, Cu_5FeS_4-533 and Cu_5FeS_4-553 are 120, 151 and 155, respectively. Obviously, the mechanical robustness of CS bulks is more preferable than that of SS bulks.

4. Conclusion

In summary, we have for the first time shown a solution-based strategy for large-scale synthesis of p-type Cu_5FeS_4 non-stoichiometric nanocrystals and characterized the thermoelectric properties of dense materials compacted from those nanocrystals. A largely enhanced power factor is observed in our wet-chemistry nanostructured dense material due to the raised carrier density. Combined with the very intrinsic low thermal conductivity owing to the structural complexity of bornite, the peak *ZT* value reaches 0.56 at 690 K which is about 47% higher than that of the-state-of-art value for this material at similar temperature. Further enhancement of the thermoelectric properties can possibly be obtained through fine tuning of the chemical composition and better controlling the grain size during the colloidal synthesis procedure.

Acknowledgement

This work was financially supported in part by the National Natural Science Foundation of China (Grant Nos. 11404044, 51472036), the Fundamental Research Funds for the Central Universities (106112016CDJZR308808). The work conducted at the Chongqing Institute of Green and Intelligent Technology, Chinese Academy of Sciences is supported by the 100 Talent Program of the Chinese Academy of Sciences (Grant No. 2013-46), the National Natural Science Foundation of China (Grant No.51401202), and the Project for Fundamental and Frontier Research in Chongqing (CSTC2015JCYJBX0026).

References

[1] K. L. Peng, X. Lu, H. Zhan, S. Hui, X. D. Tang, G. W. Wang, J. Y. Dai, C. Uher, G. Y. Wang and X. Y. Zhou, *Energy Environ. Sci*., 9 (2016), pp. 454−460.

[2] F. J. Fan, B. Yu, Y. X. Wang, Y. L. Zhu, X. J. Liu, S. H. Yu, and Z. F. Ren, *J. Am. Chem. Soc.*, 133 (2011), pp. 15910−15913.

[3] D. F. Yang, W. Yao, Q. F. Chen, K. L. Peng, P. F. Jiang, X. Lu, C. Uher, T. Yang, G. Y. Wang, and X. Y. Zhou., *Chem. Mater.*, 28 (2016), pp. 1611−1615.

[4] X. Lu, D. T. Morelli, Y. Xia, and V. Ozolins, *Chem. Mater.*, 27 (2015), pp. 408−413.

[5] W. J. Xie, S. Populoh, K. Galazka, X. X. Xiao, L. Sagarna, Y. F. Liu, M. Trottmann, J. He, A. Weidenkaff, *J. Appl. Phys.*115 (2014), pp. 103707−103713.

[6] X. Y. Zhou, G. Y. Wang, L. Zhang, H. Chi, X. L. Su, J. Sakamoto and C. Uher, *J. Mater. Chem.*, 22 (2012), pp. 2958−2964.

[7] G. J. Snyder, E. S. Toberer, *Nat. Mater.*, 7 (2008), pp. 105−114.

[8] Y. Z. Pei, X. Y. Shi, A. LaLonde, H. Wang, L. D. Chen and G. J. Snyder, *Nature*, 473 (2011), pp. 66−69.

[9] Y. Z. Pei, H. Wang and G. J. Snyder, *Adv. Mater.*, 24 (2012), pp. 6125−6135.

[10] W. Liu, X. J. Tan, K. Yin, H. J. Liu, X. F. Tang, J. Shi, Q. J. Zhang and C. Uher, *Phys. Rev. Lett.*, 108 (2012), pp. 166601−166605.

[11] J. P. Heremans, C. M. Thrush and D. T. Morelli, *Phys. Rev. B*, 70 (2004), pp. 115334−115338.

[12] T. C. Harman, P. J. Taylor, M. P. Walsh and B. E. LaForge, *Science*, 297 (2002), pp. 2229−2232.

[13] J. P. Heremans, V. Jovovic, E. S. Toberer, A. Saramat, K. Kurosaki, A. Charoenphakdee, S. Yamanaka and G. J. Snyder, *Science*, 321 (2008), pp. 554−557.

[14] J. Eilertsen, S. Rouvimov and M.A. Subramanian, *Acta Mater.*, 60 (2012), pp. 2178–2185.

[15] K. Kishimoto, Y. Sasaki, T. Koyanagi, K. Ohoyama and K. Akai, *J. Appl. Phys.*, 111 (2012), pp. 093716–093724.

[16] B. C. Sales, D. Mandrus and R. K. Williams, *Science*, 272 (1996), pp. 1325−1328.

[17] P. F. R. Poudeu, J. D'Angelo, A. D. Downey, J. L. Short, T. P. Hogan and M. G. Kanatzidis, *Angew. Chem. Int. Edit.*, 45 (2006), pp. 3835−3839.

[18] A. J. Minnich, M. S. Dresselhaus, Z. F. Ren and G. Chen, *Energy Environ. Sci.*, 2 (2009), pp. 466−479.

[19] R. J. Korkosz, T. C. Chasapis, S. Lo, J. W. Doak, Y. J. Kim, C. I. Wu, E. Hatzikraniotis, T. P. Hogan, D. N. Seidman, C. Wolverton, V. P. Dravid and M. G. Kanatzidis, *J. Am. Chem. Soc.*, 136 (2014), pp. 3225−3237.

[20] X. Lu, D. T. Morelli, Y. X. Wang, W. Lai, Y. Xia, and V. Ozolins, *Chem. Mater.*, 28 (2016), pp. 1781–1786.

[21] H. Wang, Y. Z. Pei, A. D. LaLonde and G. J. Snyder, *P. Natl. Acad. Sci. USA*, 109 (2012), pp. 9705−9709.

[22] T. J. Zhu, C. G. Fu, H. H. Xie, Y. T. Liu, B. Feng, J. Xie and X. B. Zhao, *EPL*, 104 (2013), pp. 46003−46007.

[23] H. Lee, D. Vashaee, D. Z. Wang, M. S. Dresselhaus, Z. F. Ren and G. Chen, *J. Appl. Phys.*, 107

(2010), pp. 094308−094314.

[24] P. F. Qiu, T. S. Zhang, Y. T. Qiu, X. Shi and L. D. Chen, *Energy Environ. Sci.*, 7 (2014), pp. 4000–4006.

[25] B. A. Grguric, A. Putnis, R. J. Harrison, *Am. Mineral.*, 83 (1998), pp. 1231–1239.

[26] G. V. Laan, R. A. D. Pattrick, J. M. Charnock, B. A. Grguric, *Phys. Rev. B*, 66 (2002), pp. 045104−045108.

[27] Y. Ding, D. R. Veblen, C. T. Prewitt, *Am. Mineral.*, 90 (2005), pp. 1256–1264.

[28] F. J. Fan, Y. X. Wang, X. J. Liu, L. Wu and S. H. Yu, *Adv. Mater.*, 24 (2012), pp. 6158−6163.

[29] Q. F. Chen, G. W. Wang, A. J. Zhang, D. F. Yang, W. Yao, K. L. Peng, Y. C. Yan, X. N. Sun, A. P. Liu, G. Y. Wang and X. Y. Zhou, *J. Mater. Chem. C*, 3 (2015), pp. 12273−12280.

[30] L. D. Zhao, S. Q. Hao, S. H. Lo, C. I. Wu, X. Y. Zhou, Y. Lee, H. Li, K. Biswas, T. P. Hogan, C. Uher, C. Wolverton, V. P. Dravid and M. G. Kanatzidis, *J. Am. Chem. Soc.*, 135 (2013), pp. 7364−7370.

Table 1. Carrier density (n), mobility (μ), electrical conductivity (σ), Seebeck coefficient (S), electric lattice thermal conductivity (κ_e), lattice thermal conductivity (κ_L), average chemical composition obtained by ICP and Vickers hardness (HV) at room temperature for Cu_5FeS_4 compounds synthesized at 493 K, 533 K and 553 K.

samples	n (cm^{-3})	μ ($cm^2V^{-1}s^{-1}$)	σ (S/m)	S (μVK^{-1})	κ_e ($Wm^{-1}K^{-1}$)	κ_L ($Wm^{-1}K^{-1}$)	Average chemical composition	HV (HV50/10)
Cu_5FeS_4-493	2.6×10^{20}	3.1	12889	79	0.08	0.56	$Cu_{5.28}Fe_{0.82}S_4$	155
Cu_5FeS_4-533	1.5×10^{20}	2.6	6338	80	0.04	0.44	$Cu_{5.1}Fe_{0.89}S_4$	151
Cu_5FeS_4-553	1.4×10^{20}	2.2	4983	131	0.03	0.38	$Cu_{5.26}Fe_{0.91}S_4$	120

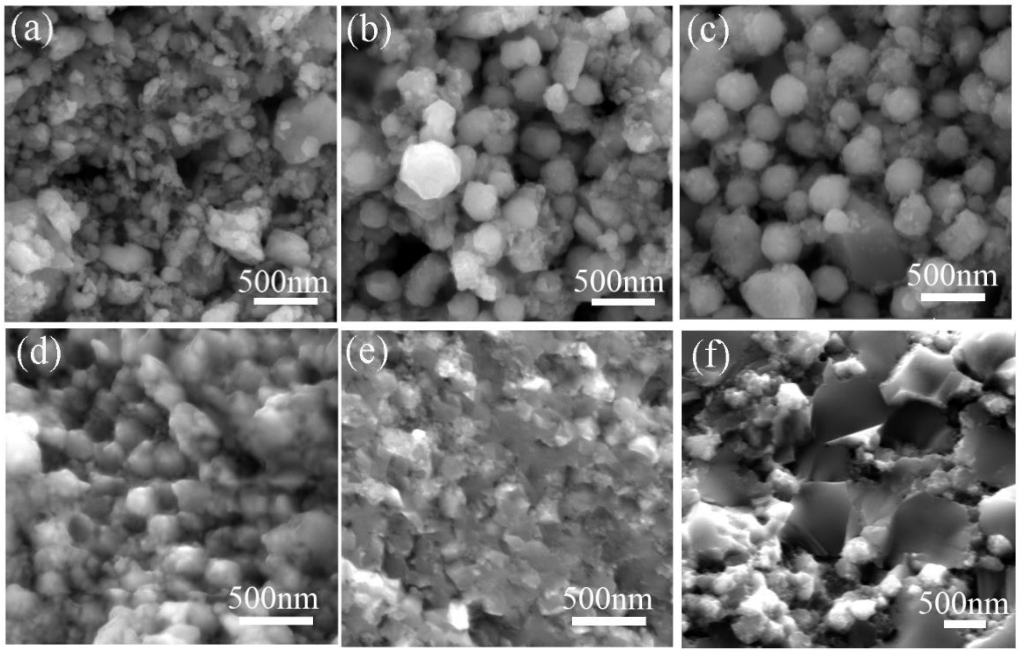

Figure 2. SEM images of Cu_5FeS_4 NCs synthesized at (a) 493 K, (b) 533 K, (c) 553 K and their corresponding bulk materials compacted by SPS are shown in (d), (e), (f).

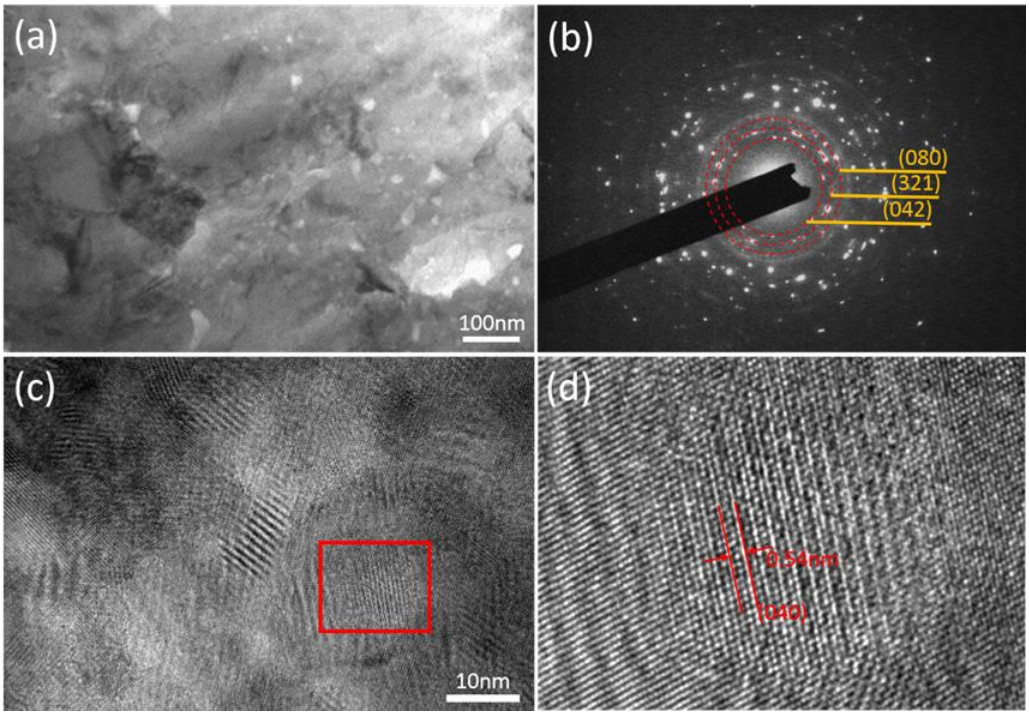

Figure 3. (a) Bright-field TEM image of the sample Cu_5FeS_4-553. (b) The corresponding selected area electron diffraction (SAED) pattern. (c) An enlarged TEM image showing many small grains. (d) High-resolution TEM image taken from the marked area in (c).

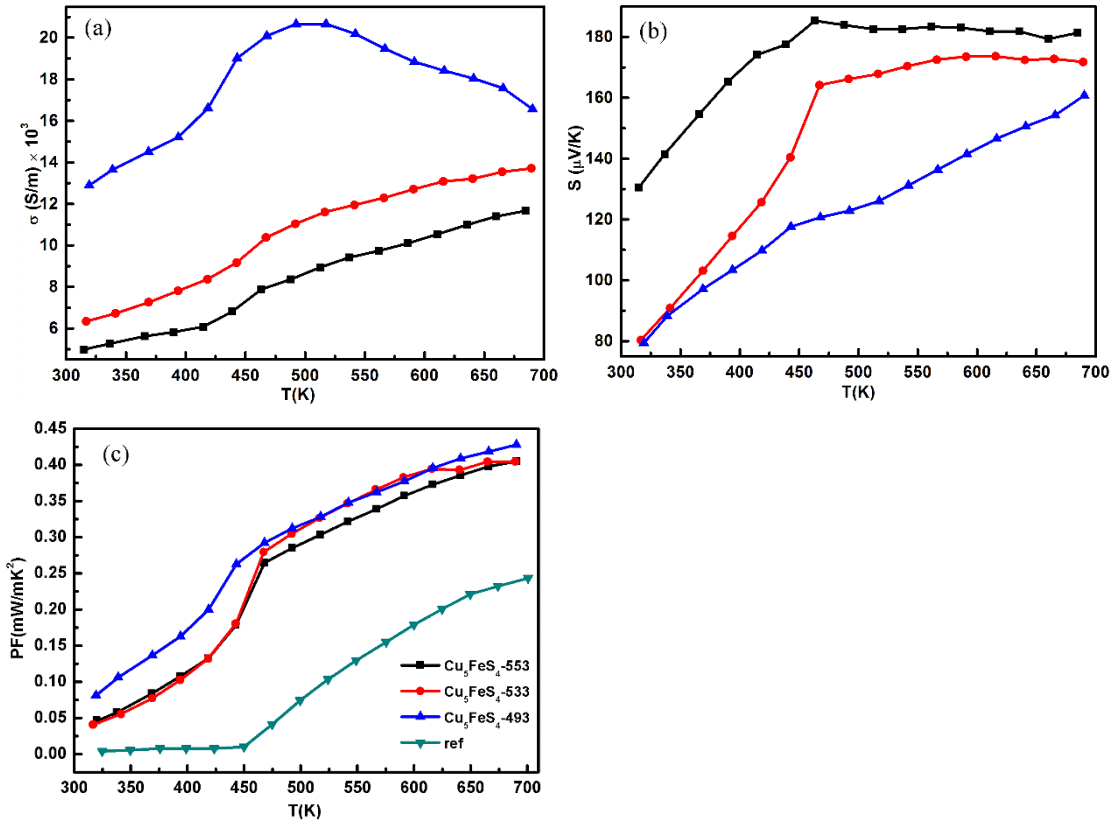

Figure 4. Temperature-dependent (a) electrical conductivities and (b) Seebeck coefficients (c) power factors for Cu_5FeS_4 compounds synthesized at 493 K, 533 K and 553 K. The *PF* of reference data is also included in (c) for comparison.

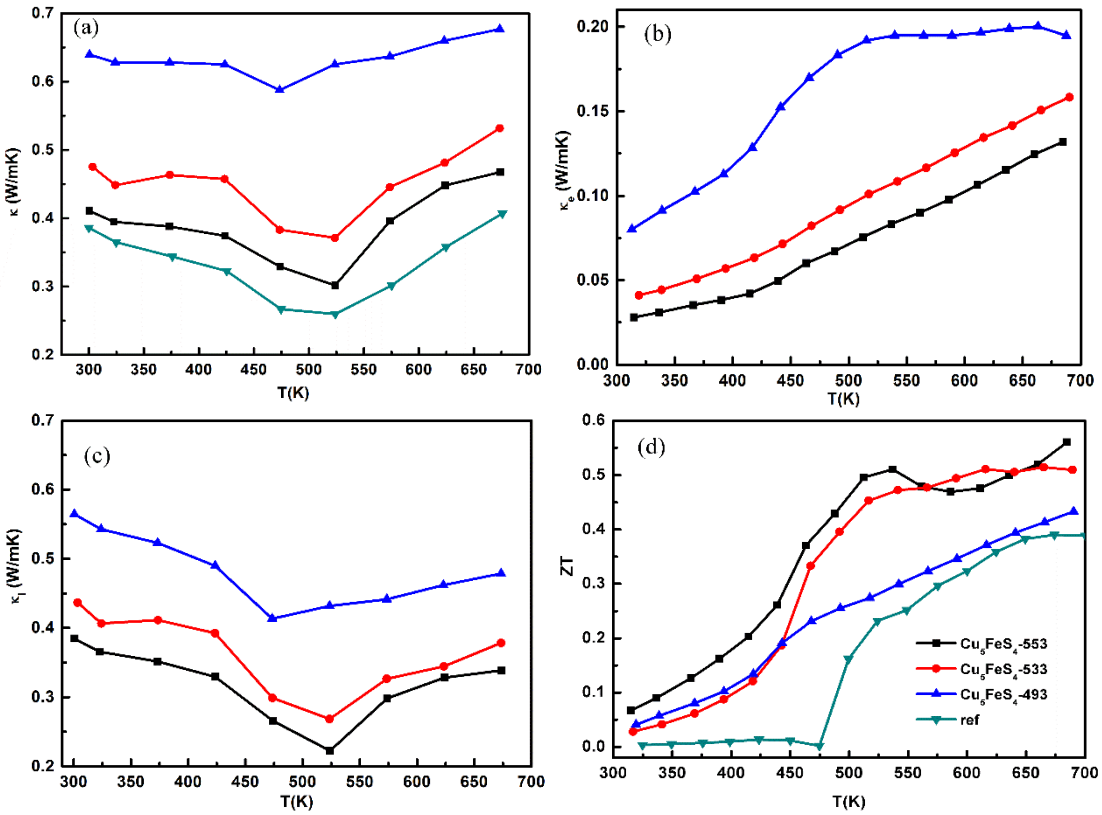

Figure 5. Temperature-dependent (a) total thermal conductivities (b) charge carrier thermal conductivities, (c) lattice thermal conductivities and (d) *ZT* values for Cu_5FeS_4 compounds synthesized at 493 K, 533 K and 553 K. The κ and *ZT* of reference data is also included in (a) and (d) for comparison.